Hindawi
Journal of Sensors
Volume 2019, Article ID 8789473, 7 pages
https://doi.org/10.1155/2019/8789473

Research Article

Preliminary Evaluation of Gaofen-3 Quad-Polarized SAR Imagery for Longbao Protected Plateau Wetland Reserve

Qiufang Wei,[1,2,3] Yun Shao ,[1,2,3] and Xiaochen Wang [1,2,3]

[1]*Institute of Remote Sensing and Digital Earth, Chinese Academy of Sciences, Beijing 100101, China*
[2]*Laboratory of Target Microwave Properties, Deqing Academy of Satellite Applications, Deqing, Zhejiang Province, 313200, China*
[3]*University of Chinese Academy of Sciences, Beijing 100049, China*

Correspondence should be addressed to Xiaochen Wang; wangxc@radi.ac.cn

Received 23 December 2018; Revised 17 June 2019; Accepted 24 July 2019; Published 20 August 2019

Academic Editor: Mohammad Haider

The Chinese Gaofen-3 (GF-3) synthetic aperture radar (SAR) satellite launched by the China Academy of Space Technology is under continuous operating mode at C-band since September 2016. The main objective of this study was to present a preliminary evaluation of GF-3 quad-polarized SAR imagery for protected wetland classification. Four scenes of GF-3 quad-polarized SAR imageries were collected in this study and analyzed systematically. Besides, the GF-2 optical imagery and in situ survey results were also collocated as reference data. It was verified that the polarized features including double bounce scattering component P_{dbl}, odd bounce scattering component P_{odd}, and volume scattering component P_{vol} from Freeman decomposition algorithm were well applied in distinguishing typical coverage of Longbao protected plateau wetland. In consideration of robustness of classifier, the method of Maximum Likelihood Classification was investigated for classification based on selected polarized features. The Kappa coefficient and overall accuracy of classification mapping are 0.75 and 82.16%, respectively, which revealed that the GF-3 quad-polarized SAR can provide a satisfying mapping for classification of Longbao protected plateau wetland.

1. Introduction

Wetland, a multifunction ecosystem on the earth, plays a key role in the human survival and environmental sustainable development. Wetland has gradually become a headline goal of ecosystem monitoring not only for evaluation of resource development, but also for maintenance of regional ecological environment [1–3]. For precise monitoring of wetland, remote sensing technology has been widely accepted by researchers with advantages of it being large-scale and cost effective [4, 5]. In the past decades, significant capability of space-borne Synthetic Aperture Radar (SAR) sensor toward wetland monitoring and observation in high spatial resolution under all-weather conditions has been revealed. Compared to single- or dual-polarized SAR, such as Canada satellite Radarsat-2 and Japan satellite Alos-2, quad-polarized SAR is occupied by more polarization status which can provide more scattering details to meet the demand of fine wetland monitoring [6–9]. Some studies revealed the capability of orbited quad-polarized SAR for wetland classification. Gou et al. [10] proposed an unsupervised method based on a three-channel joint sparse representation classification with fully polarimetric SAR (PolSAR) data. The proposed method utilized both texture and polarimetric feature information extracted from the HH, HV, and VV channels of a SAR image. Buono et al. [11] demonstrated the PolSAR capabilities to classify coastal areas of The Yellow River delta (China) by applying two well-known unsupervised classifiers, namely the H/α-based and the Freeman–Durden (FD) model-based algorithms, to a fully polarimetric SAR scene collected by using RADARSAT-2 in 2008. Recently, Chen et al. [12] proposed a novel quad-polarized SAR image classification method based on multilayer autoencoders and self-paced learning. Wang et al. [13] proposed a new classification scheme for mud and sand flats on intertidal flats by using FD and Cloude–Pottier polarimetric decomposition.

Noteworthy, the C band multipolarization SAR Gaofen-3 (GF-3) satellite was launched into a polar sun-synchronous orbit of 755 km altitude with a 26-day repeat cycle on 10 August 2016 [14, 15]. As the first Chinese civil operating

Table 1: List of quad-polarized GF-3 SAR specifications.

Satellite	Scene ID	Acquisition Time (UTC)	Pol	Resolution/m	Swaths/km
GF-3	3377378	2017-2-27	QPSI	8	30
GF-3	3741512	2017-6-6	QPSI	8	30
GF-3	3842536	2017-7-5	QPSI	8	30
GF-3	5714664	2018-11-3	QPSI	8	30

SAR platform, it is significant to make a preliminary assessment for further application. Some preliminary analysis was also undertaken recently. An et al. [16] used two GF-3 SAR imageries to extract the coastlines of the regions of Bohai and Taihu in China, respectively. Guo et al. [17] investigated the capability of quad-polarized SAR for land cover type classification using deep highway unit networks model.

Although GF-3 SAR has been operational for a period of time, only a few studies revealed its polarization capability. The application performance of GF-3 polarimetric SAR data still needs to be fully assessed. Besides, considering the significant status of GF-3 SAR in Chinese development of spaceborne SAR, it is urgent to perform capability evaluation of GF-3 SAR for different observation scenes. The main objective of this study was to demonstrate the potential of GF-3 quad-polarized SAR and present a preliminary quantitative result for wetland classification. To make an interpretation of GF-3 SAR for wetland monitoring, besides the normalized radar cross-section (NRCS) processing, the known polarization decomposition algorithms of Freeman and H/A/Alpha decomposition were further applied to four scenes of GF-3 quad-polarized SAR imageries collected over Longbao protected plateau wetland.

2. Study Area and Dataset

2.1. Study Area. Longbao protected plateau wetland (33.11–33.27°N, 96.39–96.69°E), located in Longbao town of Yushu country, Qinghai province, is a typical protected plateau wetland that is approximately 14 km long with a maximum width of about 3.5 km (Figure 1). The maximum depth of the wetland has been reported to be about 4 m; however, most part of the wetland is generally much shallow. The entire nature reserve is flanked by steep ridges that typically rise up to 750 m above the valley floor. The wetland is fed by groundwater, streams, precipitation, snowmelt, and it drains into the Yi Chu River to the northwest, a short tributary of the nearby Tongtian River.

2.2. Remote Sensing Data

2.2.1. GF-3 Quad-Polarized SAR Data. Four scenes of GF-3 quad-polarized SAR imageries were collected in this study. The main specifications of GF-3 quad-polarized SAR used are listed in Table 1. The imagery coverage of collected GF-3 SAR is shown in Figure 1, together with Longbao protected plateau wetland scope.

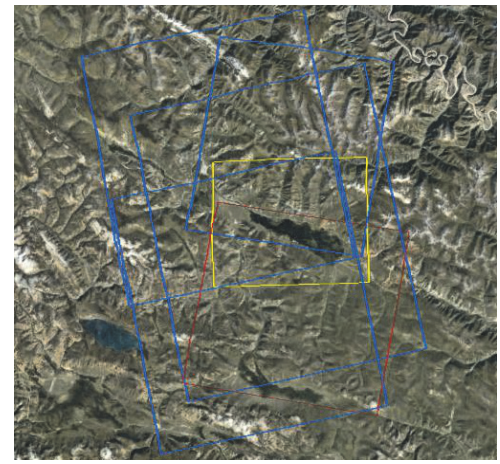

Figure 1: Imageries coverage of collected remote sensing data. Blue squares represent the GF-3 quad-polarized SAR. Red square represents the GF-2 optical imagery. Yellow square represents the Longbao protected plateau wetland scope.

2.2.2. GF-2 Optical Data. A scene of GF-2 optical imagery was collected in this study. The main specifications of GF-2 optical imagery used herein are listed in Table 2. The imagery coverage of collected GF-2 optical imagery is shown in Figure 1, together with Longbao protected plateau wetland scope.

2.2.3. In Situ Survey Data. An in situ survey for Longbao protected plateau wetland was undertaken to acquire main wetland types and ground distribution characteristics. The in situ survey route is presented in Figure 2. Four types of Longbao protected plateau wetland coverage including alpine tundra, alpine meadow, swamp meadow, and lakes were surveyed and pictured during the survey, as shown in Figure 3.

3. Experiment and Results

3.1. Selection of Polarization Features. Prior to efficient detection of change in Longbao protected plateau wetland from SAR imagery, the polarization features need to be derived from the raw polarization scattering matrix [S] according to Table 3. Twelve polarization features were proposed for statistical and comparative analysis, including three backscattering coefficients of σ_{hh}, σ_{hv}, and σ_{vv}; scattering entropy H; scattering angle α; Anisotropy A, three eigenvalues of l_1, l_2, and l_3; double bounce scattering component P_{dbl}, odd

Table 2: List of GF-2 optical specifications.

Satellite	Scene ID	Acquisition Time (UTC)	Mode	Resolution/m	Swaths/km
GF-2	5819684	2018-12-01	PMS	4	45

Table 3: The polarized features used in this study.

Polarized features	Definition
The Backscattering coefficient	$\sigma^0_{hh} = \langle S_{hh}S^*_{hh}\rangle, \sigma^0_{vv} = \langle S_{vv}S^*_{vv}\rangle, \sigma^0_{hv} = \langle S_{hv}S^*_{hv}\rangle$
Entropy	$H = \sum_{i=1}^{3} -p_i \log_3 p_i \ (p_i = \lambda_i / \sum_{j=1}^{3} \lambda_j)$
Scattering angle	$\alpha = \mathrm{p}_1\alpha_1 + \mathrm{p}_2\alpha_2 + \mathrm{p}_3\alpha_3$
Anisotropy	$\mathrm{A} = (\lambda_2 - \lambda_3) / (\lambda_2 + \lambda_3)$
Double bounce scattering component	$P_{dbl} = f_{dbl}(1 + \lvert\alpha\rvert^2)$
Odd bounce scattering component	$P_{odd} = f_{odd}(1 + \lvert\beta\rvert^2)$
Volume scattering component	$P_{vol} = (8/3)\, f_{vol}$

bounce scattering component P_{odd}, and volume scattering component P_{vol}.

Notably, the S_{hh}, S_{hv}, and S_{vv} are the elements of Sinclair matrix. λ_{i} is the i-th eigenvalue of coherence matrix $[T]$. α_{i} is derived from the i-th eigenvalue of coherence matrix $[T]$. f_{dbl}, f_{odd}, and f_{vol} are double bounce scattering, surface scattering, and volume scattering coefficients, respectively. α and β are the processed variables used to describe the relative advantages between different scattering mechanisms. $< >$ represents ensemble average, $*$ represents conjugate operation, and Re denotes real part.

In order to precisely select the optimal polarization feature or subset; radiometric calibration, geometric re-projection, and filtering de-noising operations were performed on raw SAR data. Besides, two polarization decomposition algorithms including Freeman decomposition and H/A/Alpha decomposition were applied for collection of polarization features, which are listed in Table 2. Noteworthy, all polarization features were operated under same size of de-noising window (3×3) and same coordinate system to guarantee registration in unified scale. The RGB pseudo color imageries are shown in Figure 4.

Quantitative analysis of each polarization feature was also necessary for selection of optimal polarization feature or subset. With the objective of discriminating four types of wetland coverage, each feature listed in Table 2 was investigated into change curves shown in Figure 5. Figure 5(a) exhibits that the NRCS variations of HH, HV, and VV are slightly obvious, but not enough for precisely differentiate alpine tundra, alpine meadow, swamp meadow, and lakes. For the abovementioned four types of coverages, the biggest biases of NRCS are 2.64, 1.76, and 2.14 dB, respectively, for HH, HV, and VV polarization. Moreover, the Freeman and H/A/Alpha decomposition components were also proposed in this section. Noteworthy, the decomposition components were normalized by using (1) to keep all parameters in same scale.

$$F_i = \frac{F_{\mathrm{i}}}{\sum_{\mathrm{i}=1}^{3} F_i} \tag{1}$$

Notably, F_i is the polarized features derived from Freeman and H/A/Alpha decomposition.

Figure 5(b) demonstrates that the performance of α can well differentiate lake, swamp meadow, and alpine meadow; but not alpine tundra and alpine meadow. The performance of both H and A shows similar curves for lake, swamp meadow, alpine meadow, and alpine tundra, and the characteristic of curves are not as clear as α. Figure 5(c) represents the Freeman decomposition component. A sharp curve of P_{dbl} represents the dominance of double scattering mechanism in classifying the coverages of the Longbao protected plateau wetland. Although small bias exists in the performance of P_{odd} and P_{vol}, it is still satisfying enough to differentiate lake, swamp meadow, alpine meadow, and alpine meadow with either polarized feature. Considering the impact of polarized features in Longbao protected plateau wetland mapping, it was suggested to adopt the polarized features P_{dbl}, P_{vol}, and P_{vol} from Freeman decomposition as main factors for further classification input.

3.2. Maximum Likelihood Classification. Herein, the selected polarization parameters were measured for Longbao protected plateau wetland coverage type classification. In consideration of robustness of classifier, the method of Maximum Likelihood Classification (MLC) is widely applied in polarized SAR classification [18, 19]. In this study, the MLC was selected for classification evaluation.

The steps for selected polarization features for Longbao plateau wetland classification performance are listed as follows:

(1) 80000 pixels are randomly selected as training input of classifier, among which four typical Longbao protected plateau wetland coverage includes alpine tundra, alpine meadow, swamp meadow, and lakes.

(2) The selected pixels are input into classifier with each tag of coverage type. The iteration process stops until the specified pixel is classified into a certain types of alpine tundra, alpine meadow, swamp meadow, and lakes.

(3) Another 80000 pixels are used for verification of classification performance. Owing to absence of in situ survey data, the high resolution GF-2 optical imageries are used

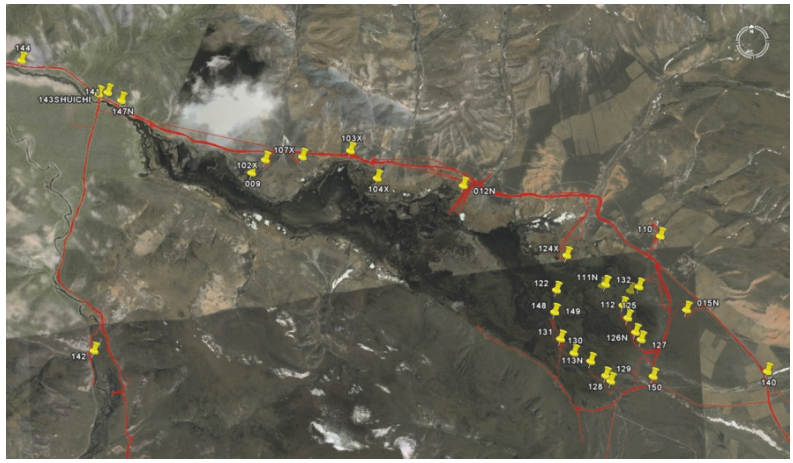

Figure 2: The in situ survey route for Longbao protected plateau wetland.

alpine tundra alpine meadow swamp meadow lakes

Figure 3: Types of Longbao protected plateau wetland coverage.

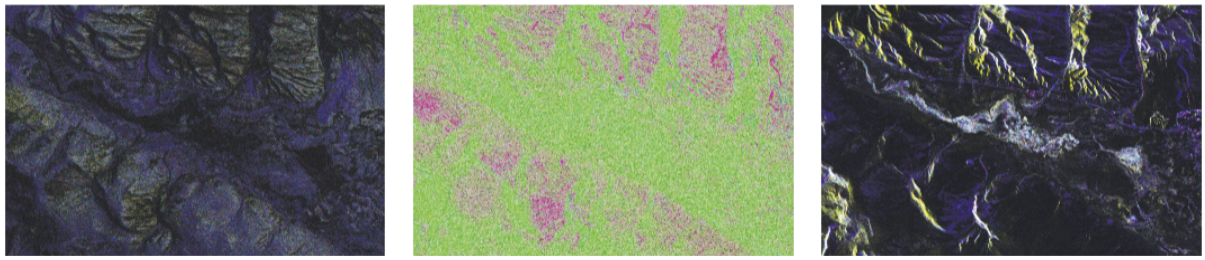

(a) (b) (c)

Figure 4: Pseudo colour imageries of raw polarization channel, Freeman decomposition and H/A/Alpha decomposition results. (a) R: σ_{hh}, G: σ_{vv}, B: σ_{hv}; (b) R: H, G:A, B: α; (c) R:P_{dbl}, G:P_{odd}, B:P_{vol}.

as reference data. Moreover, the assessment index of Kappa coefficient and average classification accuracy can be derived from confusion matrix.

(4) Operations are repeated for all three scenes of GF-3 SAR imageries. Based on the proposed Kappa coefficient and average classification accuracy, the evaluation of GF-3 quad-polarized SAR imagery for Longbao protected plateau wetland classification can be provided.

Following the abovementioned steps, the classification mapping is shown in Figure 6. Brown area represents the lakes. Yellow area represents the swamp meadow, which distributes over the lakesides. Green area represents the alpine meadow and blue area represents the alpine tundra. For further evaluation of the classification performance, the confusion matrix was derived and Kappa coefficient and mapping accuracy are presented in Table 4. Clearly, the lake (accuracy = 97.5%) is easily distinguished from other three coverage types compared to the alpine tundra (accuracy = 91.66%). The accuracy of swamp meadow and alpine meadow is 53.50 and 67.24%, respectively, which can be attributed to the similar geometric structure of these two coverage types. All in all, the overall accuracy is 82.1592% and kappa coefficient is 0.7517.

4. Discussion

Although the classification result of GF-3 quad-polarized SAR imagery for Longbao protected plateau wetland provides satisfying evaluation, a lot more systematic explorations are demanded in future study.

(1) Calibration Precision. According to the calibration formula of equation (5), the NRCS of HH, HV, VV is -26.82, -38.03, and -27.63 dB, respectively. However, the noise equivalent sigma zero (NESZ) of RADARSAT-2 standard quad-pol data is -32 dB. Considering the design parameters of GF-3 SAR,

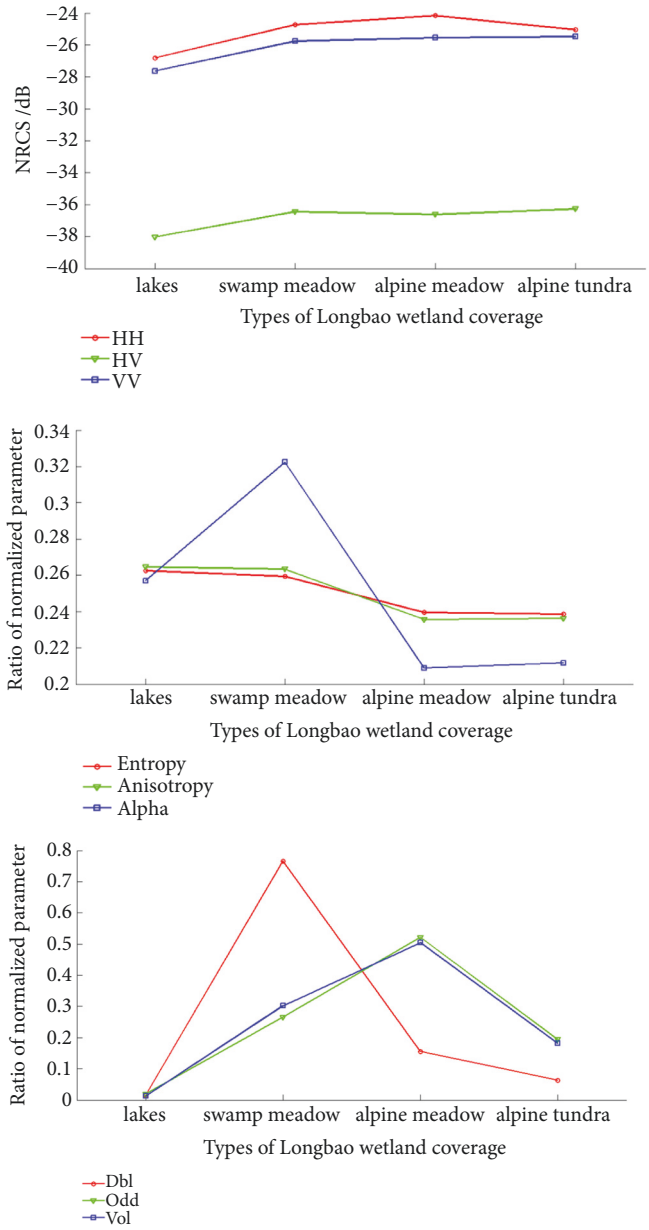

Figure 5: Polarized features response curves for different types of Longbao protected plateau wetland coverage.

Table 4: Classification performance of Longbao protected plateau wetland in 2018-07-05.

	Ground Truth (%)				
Class	Lake	Swamp meadow	Alpine meadow	Alpine tundra	Total
Lake	97.50	0.00	0.00	0.03	38.93
Swamp meadow	0.00	53.50	3.06	0.28	10.75
Alpine meadow	0.00	23.74	67.24	8.03	19.00
Alpine tundra	2.50	22.76	29.70	91.66	31.32
Total	100.00	100.00	100.00	100.00	100.00
Overall Accuracy = 82.1592%					
Kappa Coefficient = 0.7517					

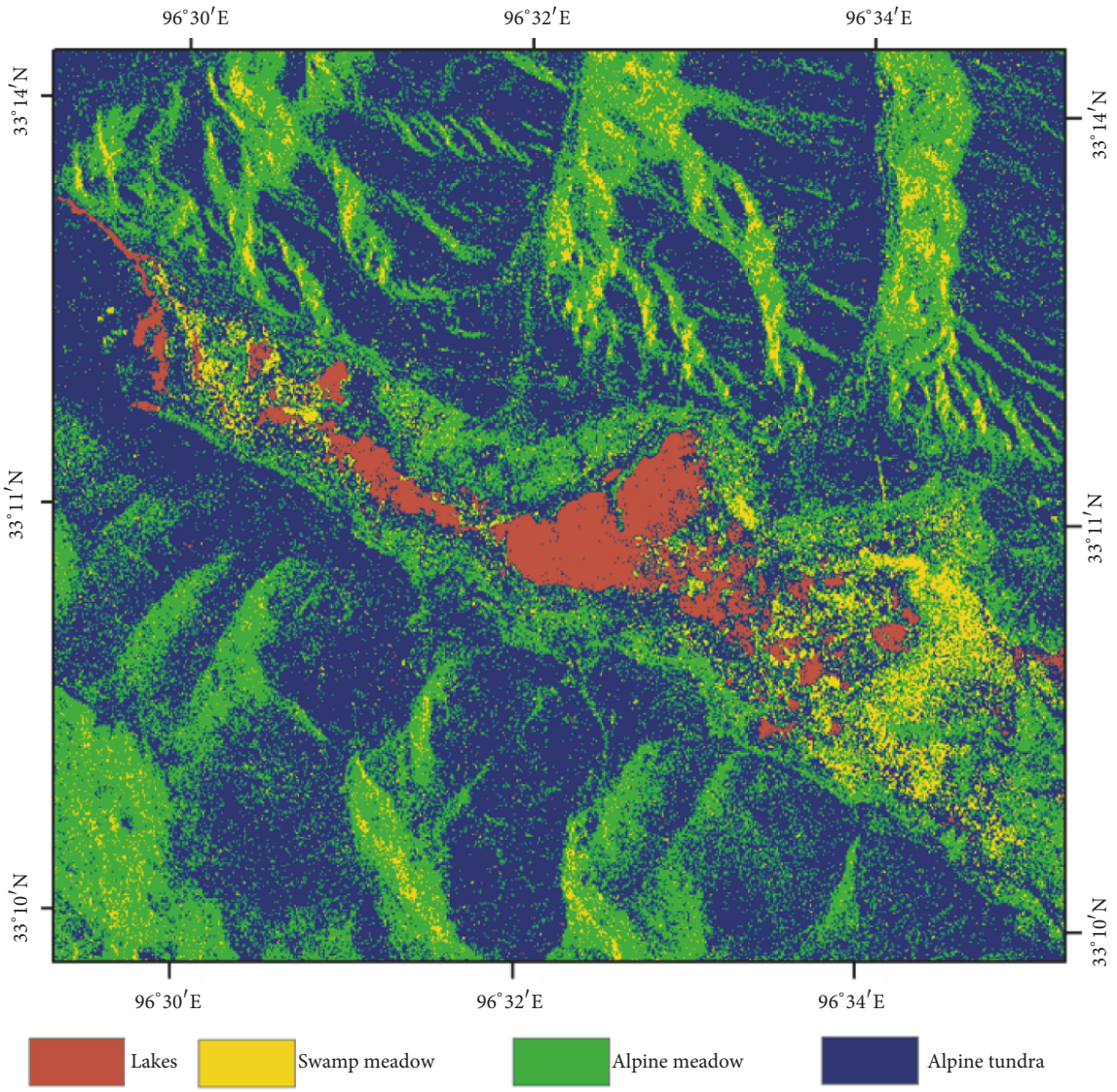

Figure 6: Classification mapping of Longbao protected plateau wetland in 2018-07-05.

there is a need to discuss and re-adjust the calibration accuracy of each polarization channel, in particular, for HV channel.

(2) Absence of Geometric Parameter of Coverages Types. Owing to the absence of geometric parameter of coverages types, in particular, the plants height above ground or water body, lake or swamp water level, and so on, only quantitative classification accuracy of lake, swamp meadow, alpine meadow, and alpine tundra are given. In future study, a detailed in situ survey will be carried out for synchronization acquisition of satellite-earth information. The difference of polarized features for different coverage types will be related to collected ground information. More polarized scattering characteristics will be revealed in order to improve the classification performance of Longbao protected plateau wetland with GF-3 quad-polarized SAR.

5. Conclusion

This study proposed a preliminary evaluation of GF-3 quad-polarized SAR imagery for Longbao protected plateau wetland classification. The main conclusions are as follows: The imaging capability of GF-3 quad-polarized SAR for Longbao protected plateau wetland was assessed from collected dataset. Beside NRCS, the Freeman and H/A/Alpha decomposition components were also investigated. Among all listed polarized features, the double bounce scattering component P_{dbl}, double bounce scattering component P_{odd}, and volume scattering component P_{vol} from Freeman decomposition algorithm dominated in distinguishing typical coverage of Longbao protected plateau wetland. Based on MLC, the Kappa coefficient and average accuracy of Longbao protected plateau wetland classification mapping were 0.75 and 82.16%, respectively. It was thus verified that the GF-3 quad-polarized

SAR can provide a satisfying mapping for wetland classification.

Data Availability

The remote sensing data used to support the findings of this study have been deposited in the China Center for Resources Satellite Data and Application repository (http://www.cresda.com/CN/).

Conflicts of Interest

The authors declare that they have no conflicts of interest.

Acknowledgments

The authors gratefully acknowledge the financial support from the National Key Research and Development Program of China (2016YFB0502504, 2016YFB0502500) and National Science Foundation of China (Grant nos. 41431174, 61471358, and 41401427). This article is partly sponsored by the Funding of Scholarship of Chinese Academy of Sciences (Grant no. Y8SY1400CX).

References

[1] C. Liquete, G. Zulian, I. Delgado, A. Stips, and J. Maes, "Assessment of coastal protection as an ecosystem service in Europe," *Ecological Indicators*, vol. 30, pp. 205–217, 2013.

[2] J. Brenner, J. A. Jiménez, R. Sardá, and A. Garola, "An assessment of the non-market value of the ecosystem services provided by the Catalan coastal zone, Spain," *Ocean & Coastal Management*, vol. 53, no. 1, pp. 27–38, 2010.

[3] K. Pike, P. Wright, B. Wink, and S. Fletcher, "The assessment of cultural ecosystem services in the marine environment using Q methodology," *Journal of Coastal Conservation*, vol. 19, no. 5, pp. 667–675, 2015.

[4] A. Niedermeier, E. Romaneeíen, and S. Lehner, "Detection of coastlines in SAR images using wavelet methods," *IEEE Transactions on Geoscience and Remote Sensing*, vol. 38, no. 5, pp. 2270–2281, 2000.

[5] B. R. Rao, R. S. Dwivedi, S. P. Kushwaha, S. N. Bhattacharya, J. B. Anand, and S. Dasgupta, "Monitoring the spatial extent of coastal wetlands using ERS-1 SAR data," *International Journal of Remote Sensing*, vol. 20, no. 13, pp. 2509–2517, 2010.

[6] X. Ding, F. Nunziata, X. Li, and M. Migliaccio, "Performance analysis and validation of waterline extraction approaches using single- and dual-polarimetric SAR data," *IEEE Journal of Selected Topics in Applied Earth Observations and Remote Sensing*, vol. 8, no. 3, pp. 1019–1027, 2015.

[7] A. Al Fugura, L. Billa, and B. Pradhan, "Semi-automated procedures for shoreline extraction using single RADARSAT-1 SAR image," *Estuarine, Coastal and Shelf Science*, vol. 95, no. 4, pp. 395–400, 2011.

[8] L. Ge, X. Li, F. Wu, and I. L. Turner, "Coastal erosion mapping through intergration of SAR and Landsat TM imagery," in *Proceedings of the 2013 33rd IEEE International Geoscience and Remote Sensing Symposium, IGARSS 2013*, pp. 2266–2269, Australia, July 2013.

[9] M. F. Bruno, M. G. Molfetta, M. Mossa, R. Nutricato, A. Morea, and M. T. Chiaradia, "Coastal observation through cosmo-skymed high-resolution SAR images," *Journal of Coastal Research*, vol. 75, no. sp1, pp. 795–799, 2016.

[10] S. Gou, X. Li, and X. Yang, "Coastal zone classification with fully polarimetric SAR imagery," *IEEE Geoscience & Remote Sensing Letters*, vol. 13, pp. 1–5, 2016.

[11] A. Buono, F. Nunziata, M. Migliaccio, X. Yang, and X. Li, "Classification of the Yellow River delta area using fully polarimetric SAR measurements," *International Journal of Remote Sensing*, vol. 38, no. 23, pp. 6714–6734, 2017.

[12] W. Chen, S. Gou, X. Wang, X. Li, and L. Jiao, "Classification of PolSAR images using multilayer autoencoders and a self-paced learning approach," *Remote Sensing*, vol. 10, no. 1, 2018.

[13] W. Wang, X. Yang, X. Li et al., "A fully polarimetric SAR imagery classification scheme for mud and sand flats in intertidal zones," *IEEE Transactions on Geoscience and Remote Sensing*, vol. 55, no. 3, pp. 1734–1742, 2017.

[14] Q. Zhang and Y. Liu, "Overview of chinese first C band multi-polarization SAR satellite GF-3," *Aerospace China*, vol. 18, no. 3, 2017.

[15] Y. Chang, P. Li, J. Yang et al., "Polarimetric calibration and quality assessment of the gf-3 satellite images[J]," *Sensors*, vol. 18, no. 2, p. 403, 2018.

[16] M. An, Q. Sun, J. Hu, Y. Tang, and Z. Zhu, "Coastline detection with gaofen-3 SAR images using an improved FCM method," *Sensors*, vol. 18, no. 6, article no. 1898, p. 431, 2018.

[17] Y. Guo, E. Chen, Y. Guo, Z. Li, C. Li, and K. Xu, "Deep highway unit network for land cover type classification with GF-3 SAR imagery," in *Proceedings of the 2017 SAR in Big Data Era: Models, Methods and Applications, BIGSARDATA 2017*, pp. 1–6, China, November 2017.

[18] M. S. Majd, E. Simonetto, and L. Polidori, "Maximum likelihood classification of single highresolution polarimetric SAR Images in urban areas," *Photogrammetrie, Fernerkundung, Geoinformation*, vol. 2012, no. 4, pp. 395–407, 2012.

[19] J. R. Otukei, T. Blaschke, and M. Collins, "Using the Wishart maximum likelihood classifier for assessing the potential of TerraSAR-X and ALOS PALSAR data for land cover mapping," *International Journal of Image and Data Fusion*, vol. 5, no. 2, pp. 138–151, 2014.